X-ray structure and biophysical properties of rabbit fibroblast growth factor 1

Jihun Lee,[a]‡ Sachiko I. Blaber,[a]‡ Andre Irsigler,[b] Eric Aspinwall[a] and Michael Blaber[a]*

[a]Department of Biomedical Sciences, College of Medicine, Florida State University, Tallahassee, FL 32306-4300, USA, and [b]Department of Biological Sciences, Florida State University, Tallahassee, FL 32306-4300, USA

‡ These authors contributed equally to this work.

Correspondence e-mail: michael.blaber@med.fsu.edu

The rabbit is an important and *de facto* animal model in the study of ischemic disease and angiogenic therapy. Additionally, fibroblast growth factor 1 (FGF-1) is emerging as one of the most important growth factors for novel pro-angiogenic and pro-arteriogenic therapy. However, despite its significance, the fundamental biophysical properties of rabbit FGF-1, including its X-ray structure, have never been reported. Here, the cloning, crystallization, X-ray structure and determination of the biophysical properties of rabbit FGF-1 are described. The X-ray structure shows that the amino-acid differences between human and rabbit FGF-1 are solvent-exposed and therefore potentially immunogenic, while the biophysical studies identify differences in thermostability and receptor-binding affinity that distinguish rabbit FGF-1 from human FGF-1.

1. Introduction

For over four decades, the rabbit has been utilized as an important animal model with which to study vascular pathology and angiogenesis, particularly involving the cornea (Brem & Folkman, 1975), hind limb (Little, 1969) and heart (Bicher & Beemer, 1967). Numerous studies of growth-factor-induced angiogenesis and arteriogenesis have utilized a rabbit model of ischemia, especially the 'hind-limb model' where ligation or excision of the femoral artery causes ischemia in the major muscles of the hind limb. A pro-angiogenic response induced in rabbit models of ischemia by exogenously added growth factors has included studies of acidic fibroblast growth factor (FGF-1; Hershey *et al.*, 2003), basic fibroblast growth factor (FGF-2; Baffour *et al.*, 1992; Landau *et al.*, 1995) and vascular endothelial growth factor (VEGF; Pu *et al.*, 1993; Takeshita *et al.*, 1995; Hershey *et al.*, 2001). Among these candidate pro-angiogenic growth factors, FGF-1 appears to be the most attractive candidate to date for angiogenic therapy and is currently in phase II clinical trials for pro-angiogenic therapy (NCT00117936; Stegmann, 2007; Stegmann *et al.*, 2000).

The amino-acid sequences of FGF-1 from a wide variety of species (including human) have been determined or have been inferred from nucleotide-sequence information; however, no cDNA or protein sequence has been reported for rabbit (*Oryctolagus cuniculus*). Two genomic sequences have been deposited for rabbit FGF-1 in the DNA database (Ensembl ENSOCUG00000013987, UniProtKB/TrEMBL B7NZB1); however, the derived amino-acid sequences from these genomic data differ from each other at a total of three positions and the inferred amino-acid sequence from the full-length genomic data differs from that of human FGF-1 at a total of four positions. We have determined a cDNA sequence for rabbit FGF-1 and have expressed recombinant rabbit FGF-1 protein, crystallized the purified protein and solved its X-ray structure to 1.80 Å resolution. We also report fundamental biophysical properties including thermostability, receptor-binding affinity and mitogenic activity, and compare these with those of human FGF-1.

2. Materials and methods

2.1. Cloning and expression

Brain tissue (cerebrum) was dissected from an 18-month-old female New Zealand white rabbit and total RNA was extracted using Trizol reagent (Invitrogen, Carlsbad, California, USA) following the manufacturer's directions. The first-strand cDNA was synthesized using Superscript III (Invitrogen) reverse transcriptase with oligo-dT as a primer. For subsequent cDNA amplification, the forward gene-specific primer (5′-ATGGCTGAAGGGGAAATCACC-3′) was designed based on multiple gene alignment of mammalian FGF-1 orthologs and the reverse primer sequence was chosen within the 3′-untranslated region of the rabbit FGF-1 genomic sequence found in the database (nucleotide positions 44367–44352 within ENSOCUG-00000013987; 5′-CAGTGCAGCCAAAGGTCAAGG-3′). PCR was carried out with PCR SuperMix High Fidelity (Invitrogen) according to the manufacturer's directions. The resulting PCR fragment was subcloned into pCR2.1 TA TOPO cloning vector (Invitrogen) and the DNA sequence was determined using the M13 forward and reverse primers (located on either side of the inserted fragment). Two independent PCR reactions were carried out using RNA isolated from different brain sections to compare the DNA sequence and minimize the potential for any PCR-based sequence artifacts.

To optimize the expression of rabbit FGF-1 in *Escherichia coli*, a synthetic gene was constructed that optimized *E. coli* codon usage; to facilitate purification, an amino-terminal six-His tag (Brych *et al.*, 2001) was also utilized (as described for human FGF-1 expressed in *E. coli*; Gimenez-Gallego *et al.*, 1986; Linemeyer *et al.*, 1990; Ortega *et al.*, 1991; Blaber *et al.*, 1996). All expression and purification followed previously published procedures for recombinant human FGF-1 (Brych *et al.*, 2001). Yields were exceptional, with >80 mg l^{-1} being produced. The purified protein was exchanged into 50 mM sodium phosphate, 100 mM NaCl, 10 mM ammonium sulfate, 2 mM dithiothreitol (DTT) pH 7.5 ('crystallization buffer') for crystallization studies, 20 mM N-(2-acetamido)iminodiacetic acid (ADA), 100 mM NaCl, 2 mM DTT pH 6.6 ('ADA buffer') for isothermal equilibrium denaturation studies, 0.14 M NaCl, 5.1 mM KCl, 0.7 mM Na$_2$HPO$_4$, 24.8 mM Trizma base pH 7.4 ('TBS buffer') for mitogenic activity assays and 10 mM HEPES, 150 mM NaCl, 3 mM EDTA, 0.05%(v/v) surfactant P20 pH 7.4 ('1× HBS-EP+ buffer') for surface plasmon resonance (SPR) studies.

2.2. Crystallization, X-ray data collection and refinement

Purified rabbit FGF-1 protein was concentrated to 10–13 mg ml^{-1} in crystallization buffer and crystals were grown using the hanging-drop vapor-diffusion method. Thin plates grew within 12 h at room temperature using a drop size of 6 µl with 0.5 ml reservoir solution containing 30% PEG 4000, 0.1 M Na HEPES pH 7.5 and 0.2 M sodium acetate. Diffraction data were collected on the Southeast Regional Collaborative Access Team (SER-CAT) 22-BM beamline (λ = 1.00 Å) at the Advanced Photon Source, Argonne National Laboratory using a MAR CCD 300 detector (MAR USA, Evanston, Illinois, USA). Crystals were mounted and cryocooled in a stream of gaseous nitrogen at 100 K. Data were integrated and scaled with *HKL*-2000 software (Otwinowski, 1993; Otwinowski & Minor, 1997).

A single monomer of His-tagged human FGF-1 (molecule *A* of PDB entry 1jqz; Brych *et al.*, 2001) was used as a search model in molecular replacement using the *Phaser* likelihood-enhanced fast rotation functions (Storoni *et al.*, 2004) implemented within the *PHENIX* software package (Terwilliger *et al.*, 2008; Zwart *et al.*, 2008). Model building and visualization utilized the *Coot* software package (Emsley & Cowtan, 2004). Structure refinement utilized the

PHENIX software package, with 10% of the data in the reflection files set aside for R_{free} calculation (Brünger, 1992). Coordinates and structure factors have been deposited in the Protein Data Bank (PDB code 3hal).

2.3. Biophysical studies

The thermodynamic parameters of rabbit FGF-1 stability were determined by isothermal equilibrium denaturation by guanidine–HCl (GuHCl) monitored by fluorescence, as previously described for recombinant human FGF-1 (Kim *et al.*, 2003). The mitogenic activity of rabbit FGF-1 was characterized using a cultured 3T3 fibroblast proliferation assay as previously described for human FGF-1 (Dubey *et al.*, 2007). FGF-1 receptor-binding studies utilized a Biacore T-100 SPR instrument (GE Healthcare, Piscataway, New Jersey, USA) at 298 K with immobilized recombinant FGF receptor 1c protein (*i.e.* the 'ligand'; FGFR1c) and soluble recombinant FGF-1 protein (*i.e.* the 'analyte'). Recombinant human FGFR1c protein was prepared as previously described (Blaber *et al.*, 2002) and was subjected to enzymatic *in vitro* biotinylation *via* the reaction of biotin ligase and D-biotin according to the manufacturer's recommendation (Avidity LLC, Aurora, Colorado, USA). The FGFR1c sensor chip was made by noncovalent capture of the biotinylated FGFR1c protein on a Series S Sensor Chip SA (GE Healthcare), with a surface-density target value of 400 response units, following the manufacturer's instructions. The reference cell surface was prepared by passing 1.0 nM D-biotin under identical conditions as for the sample cell. Recombinant human and rabbit FGF-1 proteins in serial 1:2 dilutions from 200 to 12.5 nM were injected over the sample and reference cells of the FGFR1c-SA sensor chip; for the 0 nM analyte control 1× HBS-EP+ buffer alone was injected. All runs utilized a 280 s contact time at a flow rate of 75 µl min^{-1}. At the end of analyte injection, the running buffer was passed over both flow cells at a flow rate of 50 µl min^{-1} for 180 s to monitor the dissociation phase. SPR kinetic data analysis was performed using the *Biacore T100 Evaluation* v.2.0 software package (GE Healthcare). Association (k_a) and dissociation (k_d) rate constants were determined from fitting with the 'bivalent analyte' model based upon the known X-ray structure of human FGF-1 in complex with fibroblast growth factor receptor 1 (FGFR1; PDB code 1evt; Plotnikov *et al.*, 2000).

3. Results

3.1. Rabbit FGF-1 cDNA sequence

Forward and reverse sequencing information for mRNA preparations from two different samples of rabbit brain tissue yielded identical sequence information with no ambiguous nucleotide positions (Fig. 1). With the exception of the forward PCR primer region and nucleotide position 303, the rabbit cDNA sequence is in complete agreement with genomic sequence UniProtKB B7NZB1 but not with ENSOCUG00000013987. Outside the forward PCR primer region there are a total of four amino-acid changes when comparing rabbit FGF-1 with human FGF-1. For consistency in the presentation of results and discussion these will be referenced in terms of the change from human to rabbit and include Pro20→Ala, Lys25→Leu, Asn95→Ser and Ile113→Thr in the 155-amino-acid numbering scheme. An alternatively processed form of FGF-1, known as the 140-amino-acid form, is proteolytically cleaved between residue positions Lys15 and Phe16; thus, the above differences between human and rabbit FGF-1 can also be defined as Pro5→Ala, Lys10→Leu, Asn80→Ser and Ile98→Thr. Since this is the expressed form of the recombinant protein used for all functional and bio-

physical studies, unless otherwise noted this will be the frame of reference used to number the amino-acid differences.

3.2. Crystal structure of rabbit FGF-1

The rabbit FGF-1 protein crystallized in a novel space group ($P2_1$) not previously seen for either wild-type or mutant forms of FGF-1.

The crystals diffracted to high resolution and an essentially complete data set was collected to 1.80 Å with excellent signal-to-noise and merging statistics (Table 1). The molecular-replacement search correctly placed two molecules in the asymmetric unit (with a resulting Matthews coefficient V_M of 2.09 Å^3 Da^{-1}). Initial electron-density maps were excellent, with the exception of the loop region
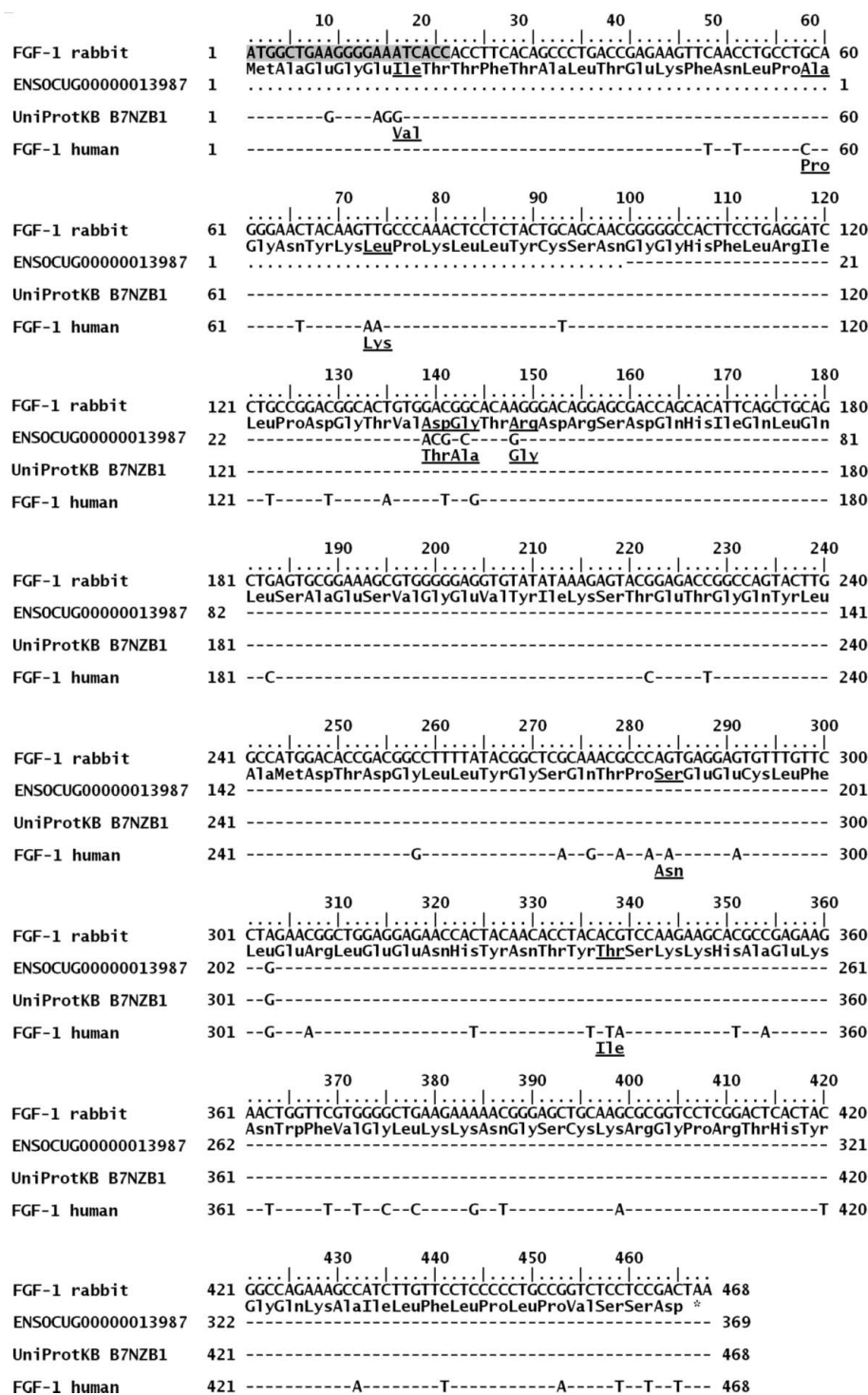

Figure 1
The rabbit FGF-1 cDNA sequence aligned with the available genomic sequences (Ensembl ENSOCUG00000013987 and UniProtKB/TrEMBL B7NZB1) and the human FGF-1 sequence (Gimenez-Gallego et al., 1986; Ensembl ENSG00000113578). The location of the forward PCR primer is indicated in gray shading. The nucleotides that differ between the rabbit FGF-1 cDNA, the genomic sequences and human FGF-1 are indicated. The amino acids that differ between the rabbit cDNA, the genomic sequences and human FGF-1 are underlined.

structural communications

involving residue positions 90–93 (*i.e.* the $\beta8$–$\beta9$ β-hairpin turn) in both molecules *A* and *B*. Manual model building of an alternative backbone conformation for this region resulted in a markedly improved agreement with the $2F_o - F_c$ electron-density map. Contiguous electron density was observed for residue positions 7–137 (referencing the 140-amino-acid numbering scheme) of both molecules *A* and *B*. No clear electron density was observed for residue positions 1–6 or the amino-terminal His tag in either molecule *A* or *B* (these positions were therefore omitted from the model coordinates). Clear difference density was present enabling unambiguous modeling of the mutations Lys10→Leu, Asn80→Ser and Ile98→Thr to complete the building of the rabbit FGF-1 structure (since no density was observed for the amino-terminus to residue position 6, the Pro5→Ala mutation could not be modeled).

Spherical positive difference density of approximately 8σ was observed adjacent to the main-chain amide and side-chain N^{ε} group of Arg119 in both the *A* and *B* molecules. The center of this density was approximately 3.5 Å distal to both N groups and was appropriately modeled by a chloride ion. Difference densities corresponding to a typically observed sulfate ion in human FGF-1 were observed adjacent to residue positions Asn18, Lys113 and Lys118 in both molecules *A* and *B* and were added to the structure. Additional minor model building involving rotamer orientations resulted in a final refined model with excellent values for the stereochemistry and Ramachandran plot and included the addition of 229 waters and 12 non-H ion atoms (involving two chloride and two sulfate ions; Table 1). The structural changes at residue positions 10, 80 and 98 (which differ between rabbit and human FGF-1), as well as the $\beta8$–$\beta9$ β-hairpin turn, are shown in Fig. 2 and described below.

3.3. Leu10

Position 10 in rabbit FGF-1 (using the 140-amino-acid numbering scheme) is a Leu residue, whereas in human FGF-1 this position is a Lys residue. An overlay of the rabbit FGF-1 X-ray structure with that of human FGF-1 (PDB code 1jqz) shows that the rabbit Leu10
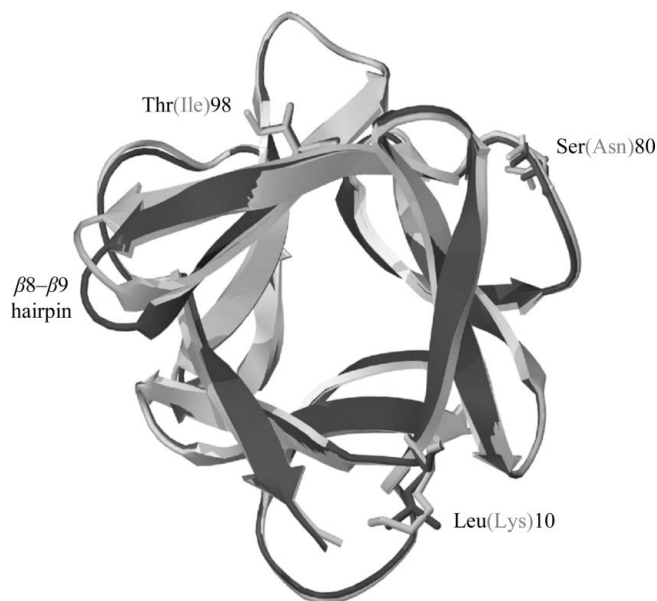

Figure 2
A ribbon diagram overlaying the rabbit FGF-1 structure (dark gray) onto the coordinates of human FGF-1 (PDB code 1jqz; light gray) and with the view down the threefold axis of pseudosymmetry. The residue positions that differ between rabbit and human FGF-1 are indicated, as is the $\beta8$–$\beta9$ turn region.

Table 1
Crystal, data-collection and refinement statistics for rabbit FGF-1.

Values in parentheses are for the highest resolution shell.

Space group	$P2_1$
Unit-cell parameters (Å, °)	$a = 49.2$, $b = 44.7$, $c = 67.1$, $\beta = 110.5$
Resolution range (Å)	50.0–1.80 (1.86–1.80)
Mosaicity (°)	0.64
Redundancy	4.3
Molecules per ASU	2
Matthews coefficient ($\text{Å}^3\,\text{Da}^{-1}$)	2.09
Total reflections	110679
Unique reflections	25636
$I/\sigma(I)$	36.1 (3.9)
Completeness (%)	99.7 (99.8)
R_{merge} (%)	6.9 (38.4)
Non-H protein atoms	2094
Solvent molecules/ions	229/12
R_{cryst} (%)	18.2
R_{free} (%)	22.7
R.m.s.d. bond lengths (Å)	0.006
R.m.s.d. bond angles (°)	0.81
Ramachandran plot†	
Favored (%)	97.7
Outliers (%)	0.0
PDB code	3hal

† Davis *et al.* (2007).

rotamer is essentially identical to that of the human Lys10 and the side-chain C^{β}, C^{γ} and C^{δ} groups of these two residues essentially overlay (Fig. 3). Thus, the Leu10 side-chain C atoms essentially follow the aliphatic C atoms of the Lys10 side chain. This residue change between rabbit and human FGF-1 at position 10 is associated with minimal structural perturbation and the local solvent structure is also retained.

3.4. Ser80

Position 80 in rabbit FGF-1 is a Ser residue, whereas in human FGF-1 this position is an Asn. An overlay of the rabbit X-ray structure with that of human FGF-1 shows a number of structural alterations associated with this residue change, principally involving details of the local hydrogen-bonding network. Considering human FGF-1 as the reference frame, the introduction of Ser80 in rabbit FGF-1 results in Glu82 breaking its hydrogen-bond interaction with Tyr74 and adopting an alternative rotamer conformation (involving a $\sim 90°$ rotation around the χ_2 angle) and subsequently forming a novel hydrogen-bond interaction with Ser80 O^{γ} (Fig. 3). The Asn80 side chain of human FGF-1 is involved in a hydrogen-bond interaction *via* solvent with the adjacent Thr78; this interaction is eliminated for the rabbit Ser80 and the intercalating solvent is displaced; a novel solvent is observed to hydrogen bond to the rabbit Ser80 O^{γ}. The main-chain amide of position 82 (forming part of a local turn structure) hydrogen bonds to Asn80 $O^{\delta1}$ of human FGF-1; however, the introduced Ser80 O^{γ} of rabbit FGF-1 is 3.5 Å distal, indicating a substantially weakened hydrogen-bond interaction, and the 82 N hydrogen-bond partner in rabbit FGF-1 is the $O^{\varepsilon1}$ group of the reoriented Glu82 side chain. The buried Cys83 side chain of human FGF-1 participates as a hydrogen-bond acceptor with the main-chain amide of position 80; however, in the rabbit FGF-1 structure the Ser side chain at position 80 becomes the primary hydrogen-bond partner for the buried Cys83 and the former 83 S^{γ}–80 N intermolecular distance increases by ~ 0.2 Å, suggesting a weakening of this hydrogen bond.

3.5. Thr98

Position 98 in rabbit FGF-1 is a Thr residue, whereas in human FGF-1 this position is an Ile. An overlay of the rabbit X-ray structure
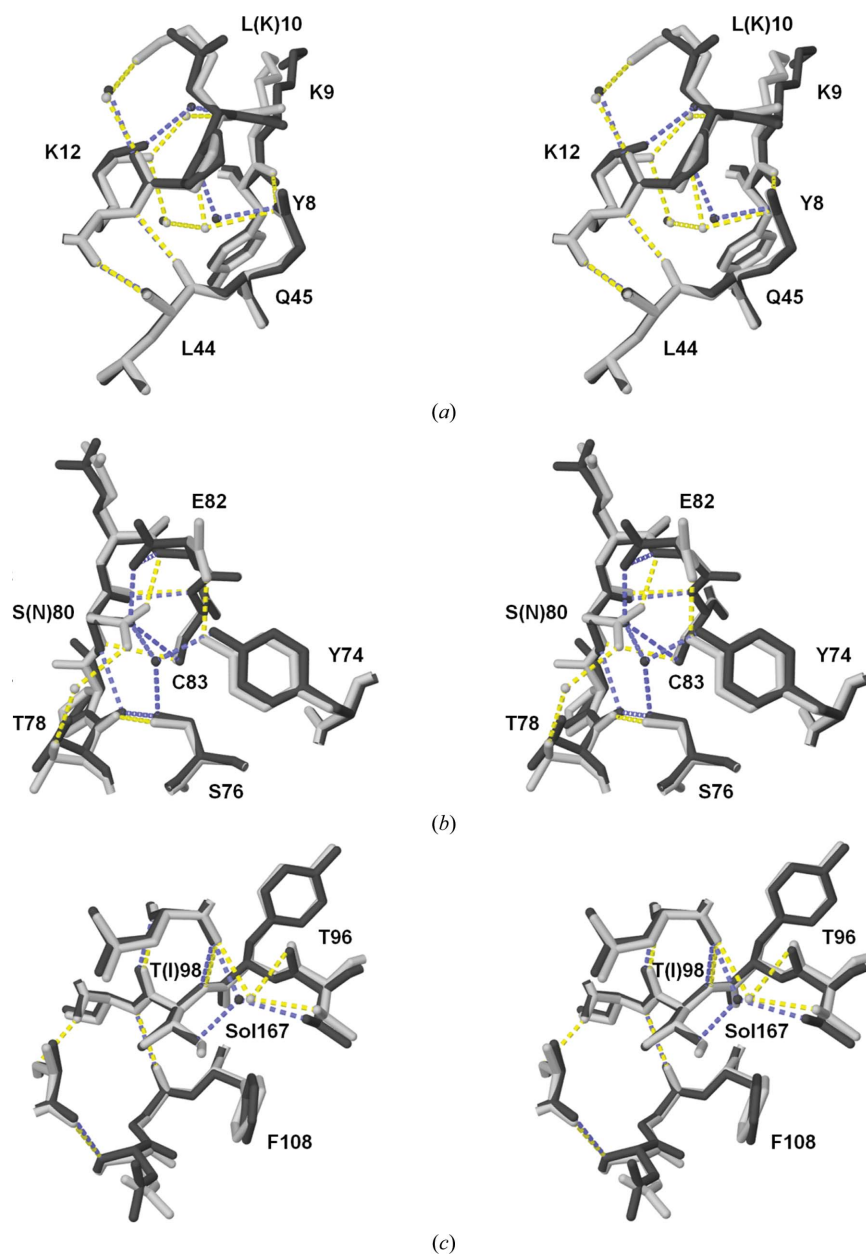
Figure 3
Relaxed stereo diagram showing an overlay of the X-ray structure of rabbit FGF-1 (dark grey) with human FGF-1 (light grey; PDB code 1jqz) at positions 10 (*a*), 80 (*b*) and 98 (*c*). These positions differ between rabbit and human FGF-1 and are visible within the X-ray structure of rabbit FGF-1. The labels indicate the residues using single-letter codes and the residues in parentheses are those of human FGF-1 at the indicated positions. Hydrogen-bond interactions in rabbit FGF-1 are indicated in blue and those in human FGF-1 are indicated in yellow.
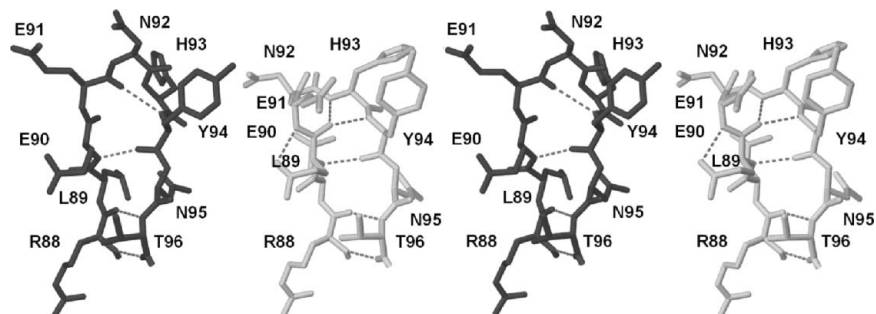
Figure 4
Relaxed stereo diagram comparing the $\beta 8$–$\beta 9$ turn region of rabbit FGF-1 (dark grey) with human FGF-1 (light grey; PDB code 1jqz). The hydrogen-bond interactions are indicated by broken lines.

Table 2
Thermodynamic parameters for rabbit FGF-1 in comparison with human FGF-1 determined by isothermal equilibrium denaturation using GuHCl.

Protein	ΔG (kJ mol^{-1})	m value (kJ mol^{-1} M^{-1})	C_m (M)	$\Delta\Delta G$† (kJ mol^{-1})
Human FGF-1‡	21.1 ± 0.6	18.9 ± 0.6	1.11 ± 0.01	—
Rabbit FGF-1	22.2 ± 0.4	21.3 ± 0.2	1.04 ± 0.01	1.4

† $\Delta\Delta G = (C_{m,human} - C_{m,rabbit})(m_{human} + m_{rabbit})/2$ as described by Pace & Scholtz (1997). A negative value of $\Delta\Delta G$ indicates a more stable mutation; the error is stated as the standard error from triple data sets. ‡ The thermodynamic parameters of human FGF-1 were previously characterized by Brych *et al.* (2003).

with that of human FGF-1 shows that these β-branched residues adopt essentially identical rotamer orientations; thus, the constituent γ atoms for both side chains overlay almost exactly (Fig. 3). The O$^{\gamma1}$ atom of the rabbit Thr residue introduces a novel hydrogen-bonding group into the position occupied by the nonpolar Ile C$^{\gamma2}$ in human FGF-1. However, an adjacent solvent molecule (Sol167) is almost ideally juxtaposed to function as a hydrogen-bond partner to the rabbit Thr. The X-ray structure indicates that this novel hydrogen-bond interaction is achieved with essentially no perturbation of the local structure (Fig. 3).

3.6. $\beta8$–$\beta9$ β-hairpin turn

The $\beta8$–$\beta9$ β-hairpin turn in human FGF-1, comprising residue positions 90–94, adopts either a type I′ 3:3 turn (PDB code 1jqz; space group $C222_1$) or a type I 3:5 turn (PDB code 2afg; space group $P2_1$; Kim *et al.*, 2002). Rabbit FGF-1, which crystallizes in the novel space group $P2_1$, adopts a uniquely different β-hairpin conformation defined as an antiparallel G1 β-bulge (Laskowski *et al.*, 1997; Fig. 4).

3.7. Biophysical properties of rabbit FGF-1

Rabbit FGF-1 has a midpoint of denaturation by GuHCl that is 0.07 M lower than that of human FGF-1 (Fig. 5), indicating that rabbit FGF-1 is slightly less stable than the human enzyme. The isothermal equilibrium denaturation data for rabbit FGF-1 fit well to the standard two-state model and yield a $\Delta\Delta G$ value of 1.4 kJ mol^{-1} in comparison to human FGF-1; thus, rabbit FGF-1 is 1.4 kJ mol^{-1} less

Table 3
Mitogenic assay of rabbit and human FGF-1 with 3T3 fibroblasts in the presence or absence of 10 U ml^{-1} heparin.

Protein	EC$_{50}$ (ng ml^{-1})		Heparin stimulation
	(−) Heparin	(+) Heparin	
Human FGF-1	58.4 ± 25.4	0.48 ± 0.08	$122\times$
Rabbit FGF-1	654.1 ± 341.6	0.26 ± 0.05	$2520\times$

Table 4
SPR data for rabbit and human FGF-1 ('analyte') with human FGFR1c D2/D3 extracellular domains ('ligand') attached to an SA chip (Biacore).

	k_a (M^{-1} s^{-1})	k_d (s^{-1})	K_d† (M)
Human FGF-1	$2.14 \pm 0.25 \times 10^6$	$17.3 \pm 1.9 \times 10^{-3}$	$8.07 \pm 0.9 \times 10^{-9}$
Rabbit FGF-1	$1.66 \pm 0.20 \times 10^6$	$19.6 \pm 2.1 \times 10^{-3}$	$11.8 \pm 0.7 \times 10^{-9}$

† Derived kinetic constants are for a global fit to all analyte-concentration data; standard deviation values are obtained from a comparison of the individual analyte-concentration fitting results.

stable than human FGF-1 (Table 2). Rabbit FGF-1 has a slightly higher folding cooperativity (m value; Table 2) in comparison to human FGF-1, thus the ΔG value extrapolated to 0 M denaturant appears slightly higher than for the human enzyme; however, ΔG values are most accurately determined at the midpoint of denaturation and therefore the $\Delta\Delta G$ value calculated by the method of Pace & Scholtz (1997) provides the most accurate analysis and is consistent with the observed perturbation of the midpoint of denaturation.

In the absence of added heparin, rabbit FGF-1 shows a demonstrable reduction in mitogenic potency in comparison to human FGF-1 in the 3T3 fibroblast cell proliferation assay (Fig. 6). The derived EC$_{50}$ values are given in Table 3 and show that rabbit FGF-1 is approximately 11 times less mitogenically active against NIH 3T3 fibroblasts than human FGF-1. In the presence of heparin the mitogenic potency of human FGF-1 increases approximately 100-fold (Fig. 6; Table 3). The response of rabbit FGF-1 to the addition of heparin shows that it is essentially indistinguishable in mitogenic activity in comparison to human FGF-1 when heparin is present (Fig. 6; Table 3).
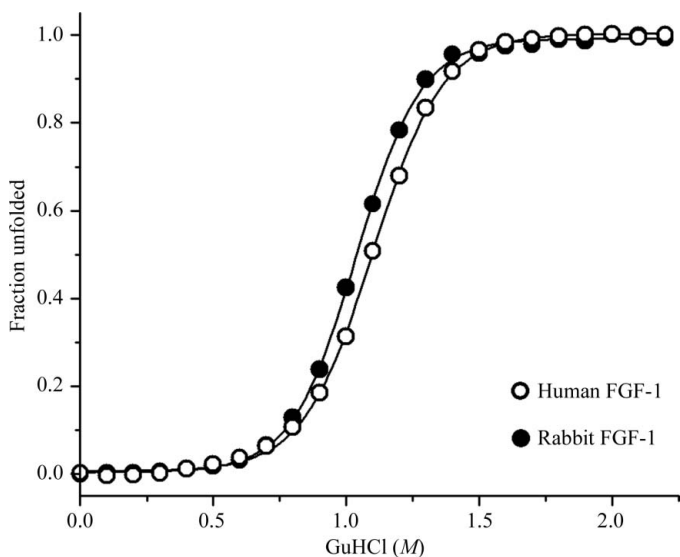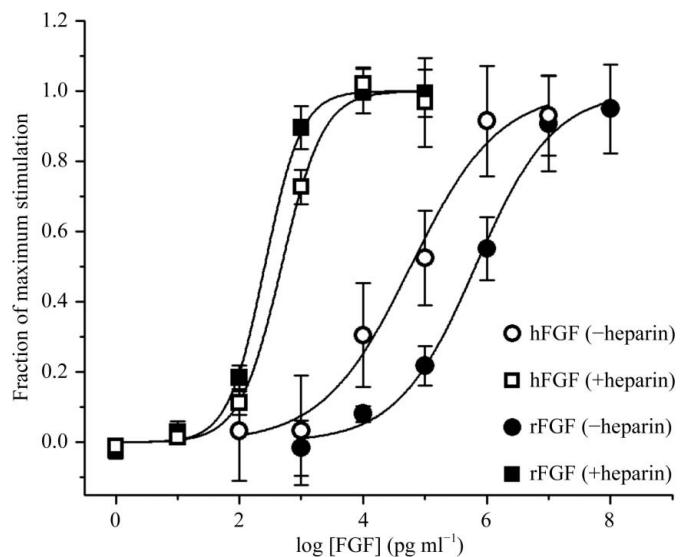

Figure 5
Fraction unfolded as a function of GuHCl denaturant concentration for rabbit and human FGF-1 as determined from isothermal equilibrium denaturation data. The derived thermodynamic parameters are provided in Table 2.

Figure 6
3T3 fibroblast cell proliferation assay for rabbit FGF-1 (rFGF) and human FGF-1 (hFGF) in the presence and absence of 10 U ml^{-1} heparin. The derived EC$_{50}$ values are given in Table 3.

The SPR sensorgrams demonstrate an excellent fit to the bivalent analyte model (Fig. 7). The derived association and dissociation rate constants (Table 4) indicate that while the dissociation rate constant k_d is essentially unchanged between rabbit and human FGF-1, rabbit FGF-1 has a slightly lower association rate constant k_a than human FGF-1. The resulting dissociation constant K_d is thus a factor of approximately 0.5-fold greater for rabbit FGF-1 in comparison to human FGF-1 (Table 4).

4. Discussion

Animal models of ischemia and angiogenesis are essential to developing effective therapies for humans and the rabbit is a *de facto* standard in this area. Furthermore, FGF-1 is emerging as a leading candidate growth factor by which permanent angiogenesis and arteriogenesis can be controllably induced. Despite its importance, the rabbit FGF-1 protein has remained essentially uncharacterized: its exact nucleotide sequence (and inferred amino-acid sequence) has remained a matter of debate and its three-dimensional structure has not been reported. Thus, important issues related to the structural basis of cross-species immunogenic potential and the biophysical/functional differences from human FGF-1 (if any) have remained unknown. To address these questions, we have determined the cDNA sequence of rabbit FGF-1, expressed the recombinant protein, solved its X-ray structure and characterized the key biophysical properties of thermostability, mitogenicity and receptor affinity.

The cDNA sequence shows nucleotide differences in rabbit FGF-1 that result in four amino-acid changes in comparison to human FGF-1 (Fig. 1). However, the forward PCR primer, designed using a consensus of mammalian FGF-1 sequences, contains a four-base-pair mismatch with a genomic sequence of rabbit FGF-1 (UniProtKB B7NZB1). Thus, we conclude that the genomic sequence within this 21-base-pair 5′-region of the rabbit FGF-1 gene is likely to represent the correct rabbit nucleotide sequence and that another amino-acid difference therefore exists between rabbit and human FGF-1 within

this region (*i.e.* Val6→Ile rabbit→human; 155-amino-acid numbering scheme). This difference is irrelevant to the 140-amino-acid form of FGF-1 used in the present study. Thus, the amino-acid differences between human and rabbit FGF-1 involve a total of either five (155-amino-acid form) or four (140-amino-acid form) amino-acid positions.

The X-ray structure of rabbit FGF-1 indicates that residue positions 1–6 (140-amino-acid numbering scheme) are disordered and thus Ala5 is highly solvent-accessible; furthermore, residue positions Leu10, Ser80 and Thr98 each exhibit solvent-accessibility of their side chains. Similar solvent-accessibilities are observed for the equivalent amino-acid positions in the crystal structure of human FGF-1 (Blaber *et al.*, 1996; Kim *et al.*, 2002). Each of these positions is therefore a potential contributor to cross-species immunogenic response between rabbit and human FGF-1.

Rabbit FGF-1 crystallized in a novel space group ($P2_1$) and therefore provides an opportunity to compare the overall structure in a novel intermolecular packing environment. While the overall molecule overlays with human FGF-1 with a root-mean-square deviation of 0.46 Å (for main-chain atoms), the $\beta8$–$\beta9$ β-turn region exhibited some notable structural alterations; this turn forms part of the binding surface with the FGF receptor in the FGF-1–FGFR1 complex (Plotnikov *et al.*, 2000). The residue changes between human and rabbit FGF-1 do not involve this turn region and therefore the alternative conformation observed in rabbit FGF-1 for this turn region are interpreted to arise from alternative crystal-packing interactions and therefore reflect intrinsic structural flexibility of this region.

The isothermal equilibrium data show that rabbit FGF-1 is 1.4 kJ mol^{-1} less stable than human FGF-1. Position 5 involves an Ala→Pro substitution when comparing rabbit with human FGF-1. In structured regions such a substitution can stabilize proteins owing to entropic destabilization of the denatured state (Matthews *et al.*, 1987); however, in situations involving natively disordered regions such a substitution is not expected to affect stability. Of the remaining positions, both the Leu10 and Thr98 side chains are accommodated
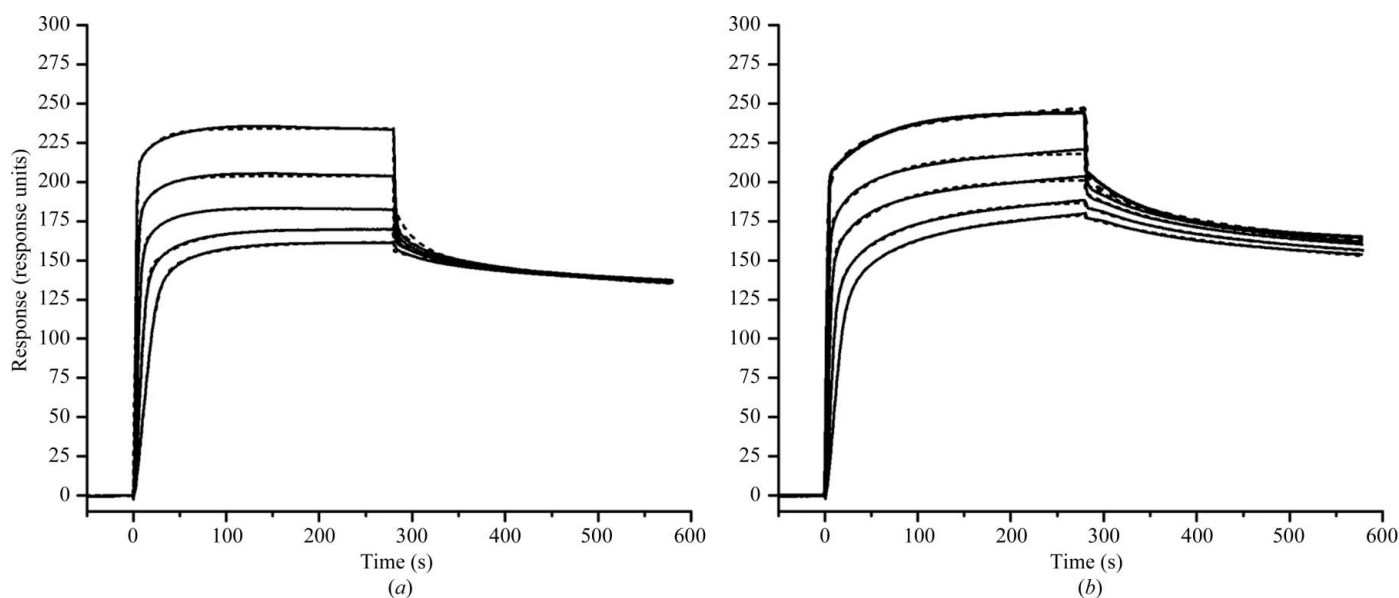

Figure 7
SPR sensorgrams (solid lines) and fitted functions (dashed lines) for rabbit FGF-1 (*a*) and human FGF-1 (*b*). The FGF-1 concentrations for the rabbit and human proteins spanned 12.5, 25, 50, 100 and 200 n*M*. In these SPR studies FGF-1 protein is the 'analyte' and the FGFR1c protein (comprising extracellular domains D2 and D3) is the 'ligand'. The FGFR1c ligand is immobilized on an SA streptavidin chip *via* biotinylation (see text for details). The fitted values of the association and dissociation rate constants and the derived K_d are given in Table 4.

structural communications

with minimal structural perturbation with reference to the alternative residues in the human FGF-1 structure, while the Ser80 residue exhibits significant changes in the local structure in comparison to Asn80 in human FGF-1. We have previously reported a structure and stability study for a series of mutations involving the adjacent conserved Cys83 residue in human FGF-1 (Lee & Blaber, 2009). These studies demonstrated that the local turn region involving residues 80–83 is both structurally rigid and optimized in its hydrogen-bond interactions (which include local main-chain amides and position 80). Thus, we conclude that the destabilization of rabbit FGF-1 in comparison to human FGF-1 is principally a consequence of the Ser substitution involving position 80.

One striking difference between rabbit and human FGF-1 is the tenfold decrease in relative mitogenic activity for rabbit FGF-1 in the absence of exogenously added heparin. Destabilizing mutations of human FGF-1 (with the exception of mutations that eliminate buried free cysteine residues) have been shown to decrease the functional half-life and increase susceptibility to proteolytic degradation (Lee & Blaber, 2009). The FGFR1c binding kinetics studies show a slightly reduced on-rate for rabbit FGF-1 in comparison to human FGF-1. However, an analysis of the available FGF-1–FGFR1 complex X-ray structure indicated that none of the amino-acid differences between rabbit and human FGF-1 involve positions that directly interact with the receptor. Therefore, it is possible that the receptor-binding kinetics for rabbit FGF-1 may be negatively affected by the reduced stability. In the presence of heparin, which stabilizes human FGF-1 and increases the melting temperature by 20 K (Copeland *et al.*, 1991), the mitogenic activities of rabbit and human FGF-1 are approximately equivalent. Thus, the destabilization of rabbit FGF-1 in comparison to human FGF-1 may contribute to the observed reduction in mitogenic activity in the absence of heparin and *in vitro* receptor-binding kinetics. Under physiological conditions, where heparin is present in the extracellular matrix and also as heparan on the cell surface, the mitogenic responses of human and rabbit FGF-1 are likely to be essentially indistinguishable.

Identification of the amino-acid differences between human and rabbit FGF-1 provides an opportunity to construct a mutant form of human FGF-1 (*i.e.* Pro5→Ala, Lys10→Leu, Asn80→Ser and Ile98→Thr; using the 140-amino-acid form) that would be immunopermissive when introduced into rabbit. Separate mutations of interest in human FGF-1 could subsequently be combined within such a background and the immune response evaluated using the rabbit as the model system. Thus, preclinical animal data related to the immunogenic potential of mutant forms of human FGF-1 might be obtained.

References

Baffour, R., Berman, J., Garb, J. L., Rhee, S. W., Kaufman, J. & Friedman, P. (1992). *J. Vasc. Surg.* **16**, 181–192.

Bicher, H. I. & Beemer, A. M. (1967). *J. Atheroscler. Res.* **7**, 409–414.

Blaber, M., DiSalvo, J. & Thomas, K. A. (1996). *Biochemistry*, **35**, 2086–2094.

Blaber, S. I., Scariscbrick, I. A., Bernett, M. J., Dhanarajan, P., Seavy, M. A., Jin, Y., Schwartz, M. A., Rodriguez, M. & Blaber, M. (2002). *Biochemistry*, **41**, 1165–1173.

Brem, H. & Folkman, J. (1975). *J. Exp. Med.* **141**, 427–439.

Brünger, A. T. (1992). *Nature (London)*, **355**, 472–475.

Brych, S. R., Blaber, S. I., Logan, T. M. & Blaber, M. (2001). *Protein Sci.* **10**, 2587–2599.

Brych, S. R., Kim, J., Logan, T. M. & Blaber, M. (2003). *Protein Sci.* **12**, 2704–2718.

Copeland, R. A., Ji, H., Halfpenny, A. J., Williams, R. W., Thompson, K. C., Herber, W. K., Thomas, K. A., Bruner, M. W., Ryan, J. A., Marquis-Omer, D., Sanyal, G., Sitrin, R. D., Yamazaki, S. & Middaugh, C. R. (1991). *Arch. Biochem. Biophys.* **289**, 53–61.

Davis, I. W., Leaver-Fay, A., Chen, V. B., Block, J. N., Kapral, G. J., Wang, X., Murray, L. W., Arendall, W. B. III, Snoeyink, J., Richardson, J. S. & Richardson, D. C. (2007). *Nucleic Acids Res.* **35**, W375–W383.

Dubey, V. K., Lee, J., Somasundaram, T., Blaber, S. & Blaber, M. (2007). *J. Mol. Biol.* **371**, 256–268.

Emsley, P. & Cowtan, K. (2004). *Acta Cryst.* D**60**, 2126–2132.

Gimenez-Gallego, G., Conn, G., Hatcher, V. B. & Thomas, K. A. (1986). *Biochem. Biophys. Res. Commun.* **128**, 611–617.

Hershey, J. C., Baskin, E. P., Glass, J. D., Hartman, H. A., Gilberto, D. B., Rogers, I. T. & Cook, J. J. (2001). *Cardiovasc. Res.* **49**, 618–625.

Hershey, J. C., Corcoran, H. A., Baskin, E. P., Gilberto, D. B., Mao, X., Thomas, K. A. & Cook, J. J. (2003). *Cardiovasc. Res.* **59**, 997–1005.

Kim, J., Blaber, S. I. & Blaber, M. (2002). *Protein Sci.* **11**, 459–466.

Kim, J., Brych, S. R., Lee, J., Logan, T. M. & Blaber, M. (2003). *J. Mol. Biol.* **328**, 951–961.

Landau, C., Jacobs, A. K. & Haudenschild, C. C. (1995). *Am. Heart J.* **129**, 924–931.

Laskowski, R. A., Hutchinson, E. G., Michie, A. D., Wallace, A. C., Jones, M. L. & Thornton, J. M. (1997). *Trends Biochem. Sci.* **22**, 488–490.

Lee, J. & Blaber, M. (2009). *J. Mol. Biol.* **393**, 128–139.

Linemeyer, D. L., Menke, J. G., Kelly, L. J., Disalvo, J., Soderman, D., Schaeffer, M.-T., Ortega, S., Gimenez-Gallego, G. & Thomas, K. A. (1990). *Growth Factors*, **3**, 287–298.

Little, R. A. (1969). *Postgrad. Med. J.* **45**, 559–561.

Matthews, B., Nicholson, H. & Becktel, W. (1987). *Proc. Natl Acad. Sci. USA*, **84**, 6663–6667.

Ortega, S., Schaeffer, M.-T., Soderman, D., DiSalvo, J., Linemeyer, D. L., Gimenez-Gallego, G. & Thomas, K. A. (1991). *J. Biol. Chem.* **266**, 5842–5846.

Otwinowski, Z. (1993). *Proceedings of the CCP4 Study Weekend. Data Collection and Processing*, edited by L. Sawyer, N. Isaacs & S. Bailey, pp. 56–62. Warrington: Daresbury Laboratory.

Otwinowski, Z. & Minor, W. (1997). *Methods Enzymol.* **276**, 307–326.

Pace, C. N. & Scholtz, J. M. (1997). *Protein Structure: A Practical Approach*, edited by T. E. Creighton, pp. 299–321. Oxford University Press.

Plotnikov, A. N., Hubbard, S. R., Schlessinger, J. & Mohammadi, M. (2000). *Cell*, **101**, 413–424.

Pu, L.-Q., Sniderman, A. D., Brassard, R., Lachapelle, K. J., Graham, A. M., Lisbona, R. & Symes, J. F. (1993). *Circulation*, **88**, 208–215.

Stegmann, T. J. (2007). *Good Clin. Pract. J.* **14**, 21–24.

Stegmann, T. J., Hoppert, T., Schlurmann, W. & Gemeinhardt, S. (2000). *Cardiac Vasc. Regen.* **1**, 5–9.

Storoni, L. C., McCoy, A. J. & Read, R. J. (2004). *Acta Cryst.* D**60**, 432–438.

Takeshita, S., Rossow, S. T., Kearney, M., Zheng, L. P., Bauters, C., Bunting, S., Ferrara, N., Symes, J. F. & Isner, J. M. (1995). *Am. J. Pathol.* **147**, 1649–1660.

Terwilliger, T. C., Grosse-Kunstleve, R. W., Afonine, P. V., Moriarty, N. W., Zwart, P. H., Hung, L.-W., Read, R. J. & Adams, P. D. (2008). *Acta Cryst.* D**64**, 61–69.

Zwart, P. H., Afonine, P. V., Grosse-Kunstleve, R. W., Hung, L.-W., Ioerger, T. R., McCoy, A. J., McKee, E., Moriarty, N. W., Read, R. J., Sacchettini, J. C., Sauter, N. K., Storoni, L. C., Terwilliger, T. C. & Adams, P. D. (2008). *Methods Mol. Biol.* **426**, 419–435.